Frequency-domain mapping approach of stability bounds for loop shaping of bilateral controllers

G. Evers, G.J.L. Naus, M.J.G. van de Molengraft, M. Steinbuch*
Eindhoven University of Technology

ABSTRACT

Bilateral control architectures include multiple control elements. In general, the relation between a single control element and the stability of the entire system is non-linear. Therefore, stability is standard evaluated a posteriori, rendering the control design process to be complex and highly iterative. A priori understanding of stability constraints would simplify the design of control elements and, as performance is fundamentally limited by stability, could provide specific guidelines whether and how performance of the bilateral teleoperation system can be optimized. This paper presents a numerical visualization method that enables stability-based control design using classical loop-shaping techniques: Frequency-domain Mapping of Bilateral Stability (FMBS). Unlike current stability-based control design approaches, the FMBS method i) is not limited to a fixed control element, a fixed control architecture or system dynamics and ii) enables the implementation of all often used stability criteria. The advantages of the FMBS method are theoretically validated through the use of two test cases, extracted from literature. Using the FMBS method, it is shown that control elements can be redesigned to achieve superior performance.

KEYWORDS: Haptics, Bilateral control, Stability, Passivity, Loop Shaping, Bode diagram.

INDEX TERMS: Haptic interfaces.

1 INTRODUCTION

A teleoperation system allows a human operator to manipulate an environment from a distance. Standard, teleoperation systems consist of a master, a communication channel and a slave. The master is controlled by the human operator and regulates the slave through the communication channel. A bilateral teleoperation system includes the feedback of the interaction force between the slave and its environment to the master. This so-called haptic feedback contributes to the perception of manipulating the environment directly. Current applications of teleoperation systems include remote handling, e.g., for nuclear waste or during space exploration, and surgery, e.g., minimally invasive surgery [1].

Generally, for a given master and slave, the communication channel is designed to optimize performance of the system while guaranteeing stability. The performance of a bilateral teleoperation system is most commonly measured in terms of the ability of the teleoperation system to present the dynamics of the environment to the human operator, so-called "transparency" [2],[3],[4]. The stability of a bilateral teleoperation system, i.e., bilateral stability, is evaluated for time-varying or for time-invariant control architectures. For time-varying control architectures, time-domain passivity control can be used [5],[6]. The most used stability criteria for time-invariant control architectures are Raisbeck's passivity, Llewellyn's absolute stability, Bounded Environment Passivity (BEP) [7] and the Nyquist criterion [2], [8]. In this paper, focus lies on time-invariant control architectures.

Figure 2 presents a general bilateral control scheme. The bilateral control architecture consists of 8 control elements $C_i(j\omega)$, for $i \in \{1, \dots, 6, m, s\}$ and where ω is frequency and j denotes the complex number [9]. The influence of a single control element to the aforementioned stability criteria is non-linear [2], [7], [8]. Standard, due to this non-linear influence, bilateral stability is evaluated after the control element has been designed, i.e., a posteriori stability evaluation. This leads to a complex and iterative design procedure for each control element. In addition, as stability fundamentally limits performance, not understanding the non-linear influence of the control element on stability generally leads to sub-optimal performance [2], [4], [7], [8], [10].

To design control elements that will contribute to a stable teleoperation system with optimal performance, methods have been developed that use stability constraints to design control elements, i.e., stability-based control design instead of a posteriori stability evaluation. Two types of stability-based control design can be distinguished: H_∞-synthesis and loop-shaping.

This paper focuses on loop-shaping based methods. Application of H_∞-synthesis to bilateral control is often complex [11] and implementation is difficult due to the loss of insight in the correlation between defined weighting functions and the resulting control elements. Also, if the designer has much insight into the design problem, H_∞ might be unnecessary for optimization [11].

In current literature, two loop shaping approaches exist that enable a stability-based control design. First, stability can be formulated in terms of an unknown control parameter, e.g., scaling factors, cut-off frequencies for low-pass filters or injected damping [4], [7], [8]. With such formulations, the control parameters are chosen to optimize performance while guaranteeing stability. Second, based on a given control architecture and stability criterion, recommendations are provided for the magnitude and the phase of a single control element. Hence, classic loop shaping techniques can be applied to design this control element [2], [12].

However, these control design methods are not generic, i.e., they are restricted to only one type of control element within one type of control architecture and for a particular set of master and slave dynamics. Moreover, loop-shaping approaches have been found only for the most simple subset of all bilateral teleoperation systems [2], [7], [8], [12]. The available methods cannot be applied to more complex control architectures or higher order master and slave dynamics.

*{g.evers, g.j.l.naus, m.j.g.v.d.molengraft, m.steinbuch}@tue.nl
Department of Mechanical Engineering, Control Systems Technology Group, P.O. Box 513 5600 MB Eindhoven

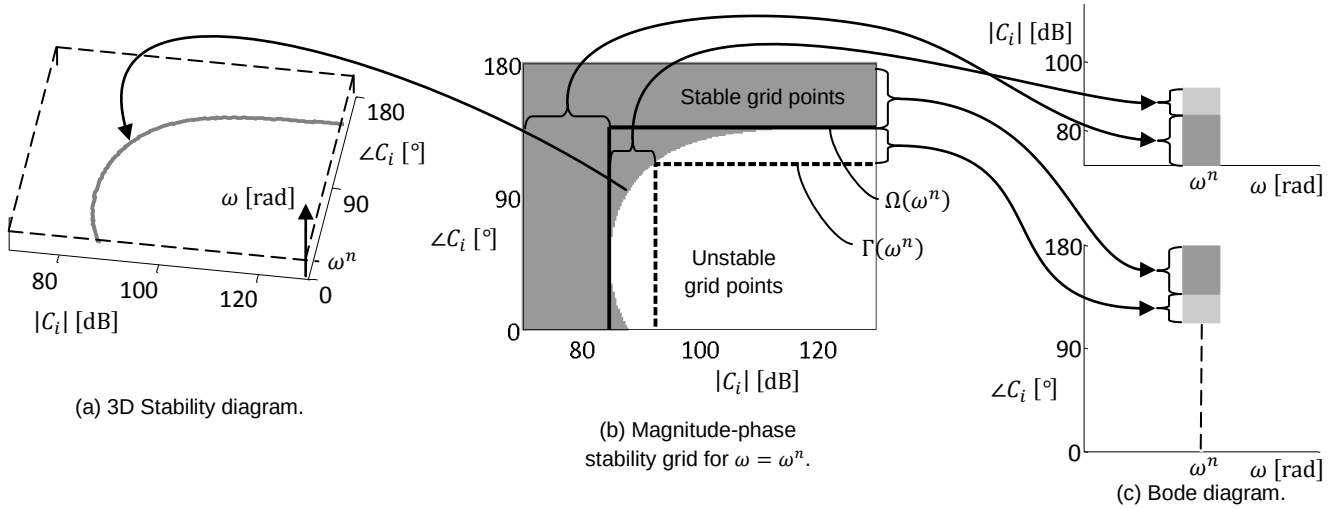

(a) 3D Stability diagram.

(b) Magnitude-phase stability grid for $\omega = \omega^n$.

(c) Bode diagram.

Figure 1: Mapping of the frequency-dependent magnitude-phase stability grid (b) onto a 3D stability diagram (a) and onto a Bode diagram (c). The solid and dotted rectangles (in b) represent the bounds on the sets $\Omega(\omega^n)$ and $\Gamma(\omega^n)$, respectively.

The contribution of this paper is twofold. Firstly, a mapping methodology is derived which is both generic and enables stability-based control design using classical loop-shaping techniques: Frequency-based Mapping of Bilateral Stability (FMBS). The FMBS method enables both the implementation of a variety of stability criteria and the application to any control architecture, any LTI control element, and LTI master and slave dynamics. Secondly, the FMBS method is applied to two test cases from literature, improving upon the existing performance, thus demonstrating the advantage of using the FMBS method.

The FMBS method is explained in Section 2. In Section 2.5, the FMBS method is applied to two test cases extracted from literature, hereby optimizing performance. This paper finalizes with conclusions and recommendations.

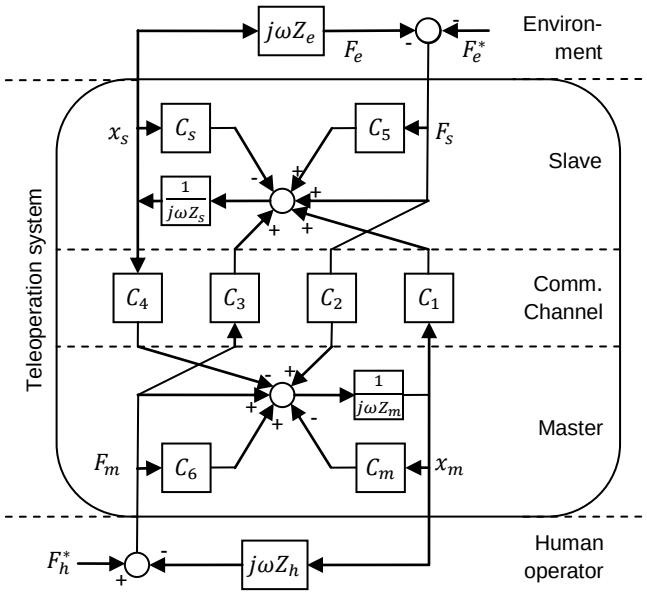

Figure 2: General bilateral control scheme [9] including C_6 and C_5. With position x_k, force F_k and impedance Z_k of the master ($k = m$), the slave ($k = s$), the environment ($k = e$) and the human ($k = h$). The superscript $*$ indicates an exogenous force. For clarity, the dependency on the Laplace operator $s = j\omega$ is omitted.

2 Frequency-based Mapping of Bilateral Stability

The Frequency-based Mapping of Bilateral Stability (FMBS) method is a mapping methodology that provides stability-based control design recommendations for a single control element $C_i(j\omega)$, enabling classical loop-shaping techniques. A generic frequency-based approach is used, allowing the evaluation of each single control element $C_i(j\omega)$ within each LTI control architecture including any LTI system dynamics, while allowing the implementation of a wide variety of often used stability criteria.

The following sections elaborate further on the FMBS method. First, the type of stability criteria that can be implemented is discussed. Second, the formulation and discretization of these stability criteria is handled, enabling a generic approach. Third, the mapping methodology that visualizes these discretized stability criteria is presented. Fourth, this visualization provides the interpretation of stability constraints in terms of classical loop shaping recommendations for an individual control element. The last section presents an overview of the FMBS approach.

2.1 Stability Criteria

Raisbeck's passivity, Llewellyn's absolute stability, Bounded Environment Passivity (BEP) and the Nyquist criterion against infinite environment stiffness are the most commonly used stability criteria for time-invariant bilateral control design. They pose requirements i) on the location of the poles of a transfer function, i.e., pole-location stability requirements, and ii) on the real and the imaginary properties of transfer functions per frequency, i.e., frequency-based stability requirements.

For Llewellyn's absolute stability, BEP and the Nyquist criterion against infinite environment stiffness, the pole-location stability requirements imply passivity of the master and the slave when they are uncoupled [3], [7], [8]. In practice, the master and the slave are passive. Hence, in general, for these stability criteria it is sufficient to evaluate the frequency-based stability requirements only.

Raisbeck's passivity includes pole-location stability requirements that evaluate effects that are dependent on the unknown control element. Nevertheless, in current literature, the pole-location stability requirements have always been satisfied (for positive impedance parameters, e.g., mass and damper of the master or slave) regardless of the control elements [7], [13].

To evaluate the pole-location dependent stability requirements, assumptions about the structure of the unknown control element are necessary. As the FMBS does not pose these assumptions, only frequency-based stability requirements are included. The pole-location stability requirements are evaluated only afterwards and only when required, e.g., for Raisbeck's passivity. The FMBS method follows a frequency-based approach which allows the implementation of all frequency-based stability requirements.

Typical examples of frequency-based stability requirements, which are used in Section 3, are the BEP criterion and the Nyquist criterion against infinite stiffness, corresponding to Eq. (1) and Eq. (2), respectively. The Nyquist criterion against infinite environment stiffness is a generalized formulation of the original stability requirement, proposed by Daniel [8],

$$\Re\{Z_{to}(j\omega)\} \geq 0, \forall\, \omega \tag{1}$$

$$\Im\left(\frac{h_{11}(j\omega)h_{22}(j\omega) - h_{12}(j\omega)h_{21}(j\omega)}{j\omega h_{11}(j\omega)}\right) < 0, \forall\, \omega \tag{2}$$

where $\Re$ and $\Im$ represent the real and imaginary part, respectively, Z_{to} is the impedance transmitted to the operator, ω is frequency, j denotes the complex number and h_{ij} are the hybrid elements,

$$Z_{to}(j\omega) = h_{11}(j\omega) - \frac{h_{12}(j\omega)h_{21}(j\omega)Z_e(j\omega)}{1 + h_{22}(j\omega)Z_e(j\omega)}, \tag{3}$$

where Z_e denotes the impedance of the environment and

$$\begin{pmatrix} F_m(j\omega) \\ v_s(j\omega) \end{pmatrix} = \begin{pmatrix} h_{11}(j\omega) & h_{12}(j\omega) \\ h_{21}(j\omega) & h_{22}(j\omega) \end{pmatrix} \begin{pmatrix} v_m(j\omega) \\ F_s(j\omega) \end{pmatrix}. \tag{4}$$

2.2 Formulation and Discretization

A priori, only one control element is unknown, whereas the remaining elements of the teleoperation system (e.g. control elements and dynamics of the master and the slave) are already defined. Therefore, the frequency-based stability requirements, e.g., Eq. (1) or Eq. (2), are formulated as a function of the frequency and the unknown – to be designed – control element $C_i(j\omega)$. As the frequency-based stability requirements depend on the real and the imaginary properties of transfer functions per frequency, no assumptions concerning the structure of $C_i(j\omega)$ are required a priori, only that it can be represented in terms of a real and imaginary part per frequency. The frequency-based stability requirements can be examined analytically or numerically. Currently, only the simplest cases have been examined analytically successfully and these approaches require assumptions about $C_i(j\omega)$ a priori [4], [7], [8]. To enable the evaluation of more complex bilateral control architectures without having to pose these assumptions, a numerical approach is taken.

The real and the imaginary part of a control element $C_i(j\omega)$ are represented by the magnitude $M_i(\omega)$ and the phase $p_i(\omega)$, i.e., $C_i(j\omega) = M_i(\omega)e^{jp_i(\omega)}$. The magnitude and the phase can be straightforwardly tuned through classical loop-shaping techniques. Therefore, understanding the stability constraints in terms of the magnitude $M_i(\omega)$, the phase $p_i(\omega)$ per frequency ω results to loop-shaping recommendations per frequency.

The numerical approach of the FMBS method requires the discretization of the frequency ω, the unknown magnitude $M_i(\omega)$ and the unknown phase $p_i(\omega)$ in N_ω, N_M and N_p discretization points, respectively. The phase range is subdivided linearly and the magnitude and the frequency ranges are subdivided logarithmically. For each frequency ω^n, where $n \in (1,2,..N_\omega)$, the evaluation of the discretized frequency-based stability requirements leads to a 2D magnitude-phase stability grid, consisting of stable and unstable grid points. This grid is shown in Figure 2.b.

Inherent to discretization, only a bounded number of points is discussed for a bounded range. For the choice of these ranges, there are two guidelines. First, similar to the plotting of a Nyquist diagram, the frequency range should be chosen large enough to cover all frequencies for which constraints on stability exist. If any control element exists that leads to a stable teleoperation system, the frequency range in which stability constraints are present is, in practice, confined. Second, the magnitude and the phase of the – to be designed – control element $C_i(j\omega)$ should lie in the user-defined magnitude range and phase range, respectively, for the entire frequency range. As the magnitudes and the phase of $C_i(j\omega)$ are unknown a priori, these ranges might have to be adapted during the loop-shaping process. In this case, based on the known phase and magnitude of the designed control element, these ranges can be adapted straightforwardly. The choice for these ranges are based on user expertise, e.g., it is known that, typically, control elements that concern position control, e.g. $C_1(j\omega)$ and $C_s(j\omega)$ have a much larger magnitude than control elements that deal with force control, e.g. $C_2(j\omega)$ and $C_5(j\omega)$.

The FMBS method evaluates whether the discretized formulation is an accurate representation of the actual stability boundaries. If the discretized function is said to be smooth, one can assume that in between two subsequent stable or unstable grid points the actual function is also stable or unstable, respectively. The level of smoothness depends on the choice for the number of discretization points: more discretization points leads to more smoothness. The FMBS evaluates the smoothness in terms of frequency, magnitude and phase using smoothness indicators [14].

2.3 Mapping Methodology

A mapping methodology is required to visualize the 2D magnitude-phase stability grid of Figure 2.b. Two mapping methodologies are applied in parallel: a 3D mapping approach and a 2D mapping approach. As both mapping methodologies present the frequency-based stability requirement in terms of the phase and the magnitude of the unknown control element $C_i(j\omega)$, interpretation of the discretized frequency-based stability requirements in terms of classical loop shaping recommendations is straightforward.

The 3D mapping approach is straightforward. First, per frequency, the boundary between stable and unstable grid points is found, see Figure 2.b. Hereafter, this boundary is mapped onto the magnitude-phase plane for that particular frequency in a 3D stability diagram, shown in Figure 2.a. Hence, the 3D stability diagram is an exact representation of the magnitude-phase stability grid.

In parallel, a 2D mapping approach is used. With respect to the 3D stability diagram, the 2D mapping approach is less complex due to its 2D format. The 2D mapping approach of the FMBS method maps the magnitude-phase stability grid onto a Bode diagram. A Bode diagram consists of a separate plot for the phase and the magnitude. Hence, to map the boundary between stable and unstable grid points of the frequency-dependent magnitude-phase grid onto the Bode diagram, separate bounds on the phase and the magnitude are required. These separate bounds

correspond to rectangular fits, which are visualized in Figure 2.b. Hence, the Bode diagram demands the approximation of rectangular bounds on the magnitude-phase stability grid.

For the 2D mapping approach, two sets of grid points are defined: an inner set $\Gamma(\omega^n)$, approximating the unstable region, and an outer set $\Omega(\omega^n)$, approximating the stable region. The inner set is, by definition, included in the outer set, i.e. $\Gamma(\omega^n) \subseteq \Omega(\omega^n)$. The inner set $\Gamma(\omega^n)$ is maximized to include as many unstable grid points as possible, without including stable grid points. The outer set $\Omega(\omega^n)$ is minimized, including all unstable grid points, i.e., all grid points outside $\Omega(\omega^n)$ are stable grid points. The sets $\Gamma(\omega^n)$ and $\Omega(\omega^n)$ are rectangular approximations of the unstable and stable regions, such that mapping of these sets onto the Bode diagram is straightforward. The boundaries of the inner set $\Gamma(\omega^n)$ and the outer set $\Omega(\omega^n)$ are shown in the white area and the dark grey area, respectively, as illustrated in Figure 2.c. The bounds on the sets $\Gamma(\omega^n)$ and $\Omega(\omega^n)$ are determined through the evaluation of all (finite number of) rectangular approximations.

This rectangular approximation of the boundary between stable and unstable grid points is not an exact representation of the actual stability boundary and adds uncertainty. This added uncertainty is represented by the set of grid points between the inner and the outer set $\Omega(\omega^n)\backslash\Gamma(\omega^n)$. This set is shown by the light grey area shown in the Bode diagram in Figure 2.c. To minimize this uncertainty, the sets $\Omega(\omega^n)$ and $\Gamma(\omega^n)$ are chosen so $\Omega(\omega^n)\backslash\Gamma(\omega^n)$ is minimized while preserving the requirement of rectangular bounds.

2.4 Interpretation

The 3D stability diagram is an exact representation of the stability boundaries. For each frequency, a detailed representation of the stability bounds on the magnitude and the phase of the control element $C_i(j\omega^n)$ is provided. With respect to the 3D mapping approach, the 2D mapping approach leads to a more easy to understand visualization on the expense of added uncertainty. The 2D mapping approach provides more basic guidelines, whereas the 3D mapping approach can be used for the most detailed loop-shaping recommendations. In frequency regions where the 2D mapping approach adds too much uncertainty, only the 3D mapping approach can be used.

The Bode diagram resulting from the 2D mapping methodology is interpreted in loop-shaping recommendations in terms of the inner set $\Gamma(\omega^n)$ and outer set $\Omega(\omega^n)$, as follows.

1. $C_i(\omega^n) \notin \Omega(\omega^n)$: frequency-based stability requirements are satisfied. The magnitude or the phase (or both) of $C_i(\omega^n)$ lie in the dark grey area.
2. $C_i(\omega^n) \in \Gamma(\omega^n)$: frequency-based stability requirements are violated. Both the magnitude and the phase of $C_i(\omega^n)$ lie in the white area.
3. $C_i(\omega^n) \in \Omega(\omega^n)\backslash\Gamma(\omega^n)$: it is unknown whether the frequency-based stability requirements are satisfied. The magnitude of $C_i(\omega^n)$ lies in the light grey area and the phase of $C_i(\omega^n)$ lies in the white area or the light grey area (or vice versa).

To satisfy the frequency-based stability requirements, according to the Bode diagram, for the discretized ranges, $C_i(\omega^n) \notin \Omega(\omega^n)$ for $n \in (1,2,..N_\omega)$, i.e., the control element $C_i(\omega)$ should be shaped to lie in the dark grey area for either the magnitude or the phase (or both). For Raisbeck's passivity, the pole-location dependent stability requirements need to be validated a posteriori.

2.5 FMBS Method

The FMBS method enables stability-based control design using classical loop-shaping techniques. The FMBS method consists of four steps: i) given a stability criterion, a known teleoperation system and one unknown control element, the frequency-based stability requirements are formulated as a function of the frequency and the unknown control element in terms of its magnitude and its phase; ii) the frequency, the magnitude and the phase of the unknown control element are discretized. The discretized formulation of the stability criterion leads to the magnitude-phase stability grid, presented in Figure 2.b. This grid consists of discretized points that either satisfy or violate the stability criterion, so-called stable and unstable grid points, respectively; iii) these stable and unstable grid points are visualized through a 2D and a 3D mapping methodology; iv) these visualizations are easily interpreted in control design recommendations because the stable and unstable grid points are described in terms of the magnitude and the phase of a control element: properties that are easily tuned through classical loop-shaping.

3 Theoretical Validation

The visualization of stability through the FMBS method provides classical loop shaping recommendations that allow performance optimization with respect to stability bounds. In this section, it is shown that for two cases from literature, in which the desired performance is not met, the performance of the system can be increased. Following these recommendations, in Section 3.1 the PF architecture of Willaert is considered, maximizing the environment stiffness for which the teleoperation system is passive [7]. Section 3.2 discusses the optimization of the force feedback control element, $C_2(j\omega)$ [8].

3.1 Optimizing Slave Position Control on Maximum Allowable Environment Stiffness

For the first test case, the Position-Force (PF) architecture presented by Willaert is considered [7]. Originally, the slave is controlled by

$$C_1^0(j\omega) = C_s^0(j\omega) = K_D j\omega + K_P, \tag{5}$$

where $K_D = 80$ Nms^{-1} and $K_P = 4.0$ kNm^{-1}. The impedances of the master and the slave are governed by $Z_m(j\omega) = 0.64j\omega + 3.4$ and $Z_s(j\omega) = 0.61j\omega + 11$.

In addition to a single control element, the FMBS method enables the formulation of the frequency-based stability requirement into a pair of control elements too, if a relation between them exists. In this case, the slave position is controlled via the control elements. $C_1(j\omega) = C_s(j\omega)$. Consequently, the corresponding frequency-based stability criterion is formulated in terms of the phase and the magnitude of $C_1(j\omega)$ only.

Willaert targets to acquire a maximum allowable environment stiffness of $K_e^{max} = 1.5$ kNm^{-1} up to which the teleoperation system is passive according to the BEP criterion, see Eq. (2). However, the original PF architecture is only passive up to $K_e^{max} = 580$ Nm^{-1} [7].

Given an environment stiffness of $K_e^{max} = 1.5$ kNm^{-1}, Figure 3 shows the 2D mapping of the BEP criterion in terms of the control elements $C_1(j\omega) = C_s(j\omega)$. This diagram indicates that the original PF architecture is indeed active for $K_e^{max} = 1.5$ kNm^{-1}; the magnitude and the phase of the control elements $C_1^0(j\omega) = C_s^0(j\omega)$ lie in the white domain for frequencies

12 Hz $< f <$ 76 Hz. To stabilize this system, an increase in phase and/ or magnitude of $C_1(j\omega) = C_s(j\omega)$ around $f = 12$ Hz is necessary. Therefore, in addition to the PD control element, a lead-lag filter is applied with frequencies $f_{lead} = 12/\hat{f}$ and $f_{lag} = 12 \cdot \hat{f}$. This provides the required phase margin, while low-frequent tracking characteristics are maintained. The new control elements thus become

$$C_1^*(j\omega) = C_s^*(j\omega) = \frac{\frac{1}{2\pi f_{lead}} j\omega + 1}{\frac{1}{2\pi f_{lag}} j\omega + 1} (K_D j\omega + K_P). \quad (6)$$

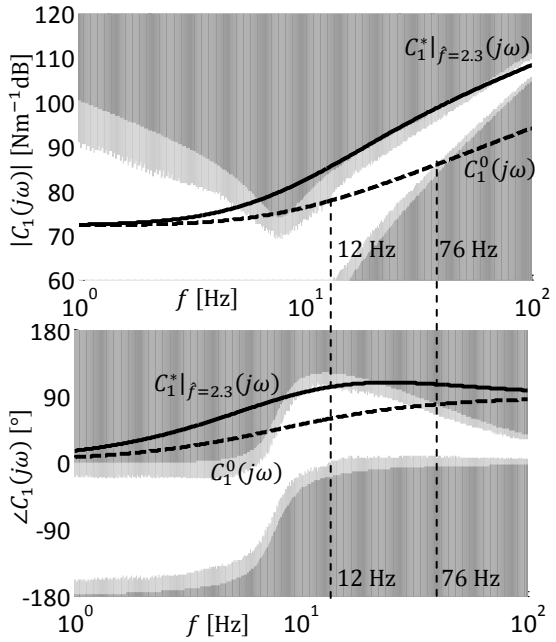

Figure 3: The 2D mapping approach evaluates passivity up to $K_e^{max} = 1.5$ kNm^{-1} in terms of $C_1(j\omega) = C_s(j\omega)$. The original control elements $C_1^0(j\omega)$ (dotted lines) and the proposed control elements $C_1^*(j\omega)$ (solid lines) violate and satisfy passivity, respectively.

For $\hat{f} = 2.3$ the resulting control elements $C_1^*(j\omega) = C_s^*(j\omega)$ satisfy the BEP criterion according to the Bode diagram. This is shown in Figure 3: $C_1(\omega^n) \notin \Omega(\omega^n)$, for $10^0 < \omega^n < 10^2$. Using the corresponding 3D stability diagram, $\hat{f}$ can be lowered to $\hat{f} = 1.7$.

3.2 Optimizing Force Feedback

The second test case discusses the Shared Compliance Control (SCC) architecture, used by Daniel [8]. The original architecture can be reformulated in terms of the control elements: $C_1(j\omega) = \frac{6\pi}{j\omega+6\pi}$, $C_5(j\omega) = 3553 \cdot \frac{7.5 \cdot 10^{-4}}{0.15 j\omega+1}$ and the force feedback control element

$$C_2^0(j\omega) = \frac{(j\omega + 4\pi)^2}{(j\omega + \pi)(j\omega + 40\pi)}. \quad (7)$$

The impedance of the master and the slave equal $Z_m(j\omega) = 1.0j\omega + 12.6 + 39.5(j\omega)^{-1}$ and $Z_s(j\omega) = 10j\omega + 377 + 3553(j\omega)^{-1}$, respectively [8]. The teleoperation system is evaluated on stability against all spring-like environments through the use of the Nyquist criterion against infinite environment stiffness.

The goal of Daniel is to design $C_2(j\omega)$ such that the Nyquist criterion is satisfied, that $C_2(j\omega) = 1$ for $f > 20$ Hz and $C_2(j\omega) = c$ for $f \to 0$ Hz, where $0 \ll c < 1$. However, the original bilateral controller violates the Nyquist criterion between $f \approx 2$ Hz and $f \approx 3$ Hz, which is shown in Figure 4. In addition, performance is limited: $0.95 < |C_2^0(j\omega)| \leq 1$ is only achieved for frequencies $f > 60$ Hz.

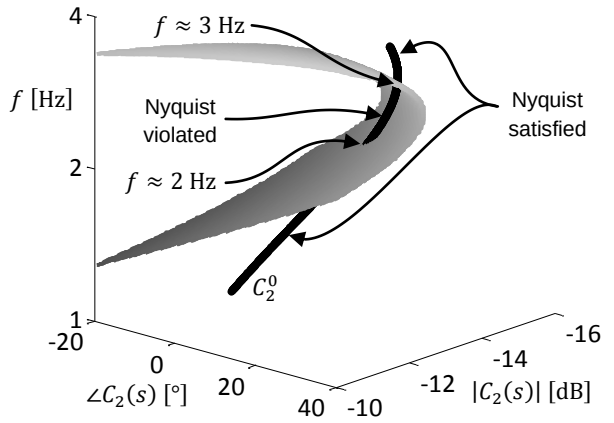

Figure 4: The 3D stability diagram of $C_2(s)$ indicates that the original control element $C_2^0(s)$ violates the Nyquist criterion.

Figure 5 illustrates the 2D mapping of the stability boundaries in terms of the control element $C_2(j\omega)$ onto a Bode diagram, indicating the aforementioned problems. Three approaches can be followed to shape $C_2(j\omega)$ to satisfy the Nyquist criterion. First, the control element can be placed inside the stable area in the phase plot for all frequencies. Second, the control element can be placed inside the stable area in the magnitude plot for all frequencies. Third, the control element can be placed in the stable phase area up to $f \approx 2$ Hz and placed in the stable magnitude area for frequencies larger than $f \approx 2$ Hz. Only the third approach is able to meet the performance requirement that $|C_2(j\omega)| = c$ in the low-frequency domain. Hence, this approach is adopted.

A second order increase in magnitude is optimal: for $f \geq 2$ Hz: a stronger increase would violate the Nyquist criterion due to the limitation of the +2 slope in the magnitude plot, whereas a weaker increase would lower the frequency at which $0.95 < |C_2(s)| \leq 1$, thereby deteriorating performance. This motivates the use of a second order lead filter with frequencies $f_{lead,1} = 2$ Hz, $f_{lag,1} = 13$ Hz.

For $f \leq 1$ Hz, negative phase is allowed. Therefore, a lag-filter can be applied to increase the low-frequent magnitude to $|C_2(j\omega)| = 1$ on the expense of a negative (allowed) low-frequent phase, using a second order lag filter with frequencies $f_{lead,2} = 2$ Hz and

$$f_{lag,2} = f_{lead,2} \frac{f_{lag,1}}{f_{lead,1}}. \quad (8)$$

Consequently, the proposed control element $C_2^*(j\omega)$ becomes

$$C_2^*(j\omega) = \left(\frac{j\omega + 2\pi f_{lead,1}}{j\omega + 2\pi f_{lag,1}} \cdot \frac{j\omega + 2\pi f_{lead,2}}{j\omega + 2\pi f_{lag,2}}\right)^2. \quad (9)$$

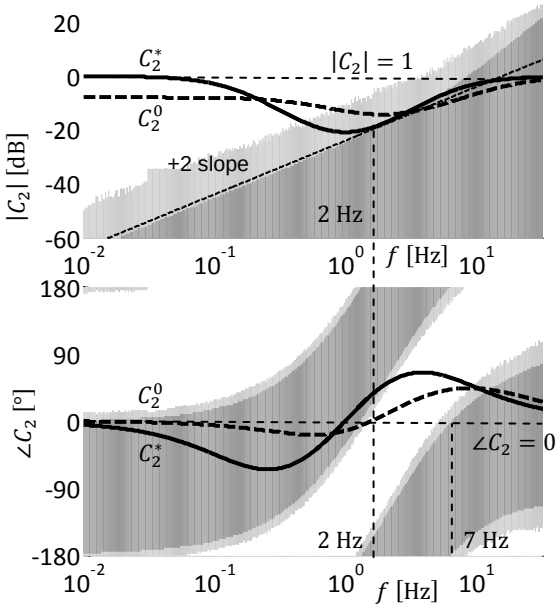

Figure 5: The 2D mapping approach indicates the regions that satisfy or violate the SIES criterion for the control element C_2. The original control element C_2^0 and the proposed control elements C_2^* are represented as the solid and dotted lines, respectively.

The improved control element $C_2^*(j\omega)$ satisfies the Nyquist criterion: Figure 5 shows that control element $C_2^*(j\omega)$ lies in the dark phase area for $f \leq 2$ Hz and lies in the dark magnitude area for $f \geq 2$ Hz. Also, performance is improved: $|C_2^*(j\omega)| \geq 0.95$ is achieved at 27 Hz, instead of 60 Hz for the original control element $C_2^0(j\omega)$.

4 Conclusion

This paper presents a control design method that enables the use of standard loop-shaping techniques for the design of a single control element $C_i(j\omega)$, while taking into account stability criteria during the loop-shaping process. The iterative nature of standard bilateral control design approaches is replaced by a straightforward stability-based design method. This iterative nature is a result of the, often highly complex, nonlinear relations between the stability criteria and the control elements. In the presented method, this nonlinear relation is reformulated and subsequently discretized in terms of the frequency and the unknown control element $C_i(j\omega)$. The unknown control element is formulated in terms of its phase and its magnitude: properties that are straightforwardly tuned through classical loop-shaping. Consequently, the presented method provides an easily interpretable translation of these nonlinear relations into control design recommendations. As performance is fundamentally limited by stability, the method provides insight in the optimality of the design of the control element for a given stability criterion.

To validate the method, two examples from literature are considered in which the desired performance is not met. In both cases, the method provides the required insight in the optimality of the original control elements with respect to the applied stability criterion. Using this insight, recommendations for redesign of the control elements are visualized by the method, allowing to improve the performance such that the desired performance can be met.

The method is generic, posing no a-priori requirements on either the bilateral controller architecture, the structure of the control element, the complexity of the teleoperation system dynamics or the stability criterion that is used. Future work includes evaluation of the method for the design of a bilateral controller for a practical setup, improved boundary approximation techniques for the 2D mapping approach and further theoretical foundation of the formulation of the frequency-based stability requirements in terms of a single control element. For each combination of stability criterion and control element, the existence of a theoretical solution can be explored, in- or excluding assumptions concerning the control architecture.

Works Cited

[1] P. Hokayem and M. Spong, "Bilateral teleoperation: An historical survey," *Automatica, vol 42, no. 12,* pp. 2035-2057, 2006.

[2] K. Fite, L. Shao and M. Goldfarb, "Loop Shaping for Transparency and Stability Robustness in Bilateral Telemanipulation," *Transactions on Robotics and Automation,* pp. 620-624, 3 June 2004.

[3] K. Hashtrudi-Zaad and S. Salcudean, "Analysis of Control Architectures for Teleoperation Systems with Impedance/Admittance Master and Slave Manipulators," *The International Journal of Robotics Research,* vol. 20, no. 6, pp. 419-445, 2001.

[4] M. Tavakoli, A. Aziminejad, R. Patel en M. Moallem, „Enhanced transparency in haptics-based master-slave systems.," in *Proceedings of the 2007 American Control Conference*, New York, 2007.

[5] M. Franken, S. Stramigioli, R. Reilink, C. Secchi en A. Macchelli, „Bridging the gap between passivity and transparency," in *Robotics: Science and Systems V*, Seattle, 2009.

[6] B. Hannaford en J. Ryu, „Time Domain Passivity Control of Haptic Interfaces," *IEEE Transactions on Robotics and Automation,* vol. 18, nr. 1, pp. 1-10, 2002.

[7] B. Willaert, B. Corteville, D. Reynaerts, H. v. Brussel and E. V. Poorten, "Bounded Environment Passivity of the Classical Position-Force Teleoperation Controller," *IEEE International Conference on Intelligent Robots and Systems,* pp. 4622-4628, 11-15 October 2009.

[8] R. Daniel and P. McAree, "Fundamental Limits of Performance for Force Reflecting Teleoperation," *The International Journal of Robotics Research,* pp. 811-830, 1998.

[9] D. Lawrence, "Stability and Transparency in Bilateral Teleoperation," *IEEE Transactions on Robotics and Automation 9-5,* pp. 624-637, 1993.

[10] A. Haddadi and K. Hashtrudi-Zaad, "Bounded-Impedance Absolute Stability of Bilateral Teleoperation Control Systems," *IEEE Transactions on Haptics,* vol. 3, no. 1, pp. 15-27, 2010.

[11] J. Yan en S. Salcudean, „Teleoperation Controller Design Using H-infinity Optimization with Application to Motion Scaling," *IEEE Transactions on Control Systems Technology,* vol. 4, nr. 3, pp. 244-258, 1996.

[12] C. Zandsteeg, D. Bruijnen and M. v. d. Molengraft, "Haptic tele-operation system control design for the ultrasound task: a loop shaping approach," *Mechatronics,* pp. 767-777, 2010.

[13] H. C. Cho en J. Park, „Impedance Controller Design of Internet-Based Teleoperation Using Absolute Stability Concept," in *IEEE Intl. Conference on Intelligent Robots and Systems*, Lausanne, Switzerland, 2002.

[14] R. Mattheij, S. Rienstra and J. t. T. Boonkkamp, Partial Differential Equations : Modeling, Analysis, Computation, Philadelphia: SIAM Press, 2005.